miR-10a-5p inhibits osteogenic differentiation of bone marrow-derived mesenchymal stem cells

YINGJIE ZHANG[1*], LISHU ZHOU[1*], ZHAOQIANG ZHANG[2*], FEI REN[3], LIANGJIAO CHEN[4] and ZEDONG LAN[5]

Departments of [1]Orthodontics, [2]Oral and Maxillofacial Surgery and [3]Oral Medicine, Stomatological Hospital, Southern Medical University, Guangzhou, Guangdong 510280; [4]Department of Orthodontics, Stomatological Hospital, Guangzhou Medical University, Guangzhou, Guangdong 510140; [5]Department of Orthodontics, Shenzhen Stomatological Hospital, Southern Medical University, Shenzhen, Guangdong 518001, P.R. China

Abstract. The use of human bone marrow mesenchymal stem cells (hBMSCs) as a tissue engineering application for individuals affected by osteoporosis and other types of bone loss diseases has been well studied in recent years. The osteogenic differentiation of hBMSCs can be regulated by a number of cues. MicroRNAs (miRNAs/miRs) serve as the key regulators of various biological processes; however, to the best of our knowledge, no information exists with regards to the specific modulatory effects of miR-10a-5p on osteogenic differentiation of hBMSCs. The aim of the present study was to investigate the relationship between hBMSCs and miR-10a-5p and, ultimately, to determine how miR-10a-5p affects the osteogenic differentiation process of hBMSCs *in vitro* and *in vivo*. The hBMSCs used in the present study were transfected with mirVana™ miRNA inhibitors and mimics, and transfection efficiency was assessed by fluorescence microscopy and reverse transcription-quantitative PCR (RT-qPCR). Viability of hBMSCs following transfection was analyzed using a Cell Counting Kit-8 assay. The mRNA expression levels of specific osteoblast markers, including alkaline phosphatase (ALP) and runt-related transcription factor 2 (RUNX2) were measured using RT-qPCR and western blot analysis. New bone formation was evaluated by Goldner's trichrome staining and micro-CT analysis *in vivo*. No significant difference in cell viability was observed among the different groups 24 h post-transfection. Overexpression of miR-10a-5p inhibited the expression of osteoblast makers in hBMSCs, whereas inhibition of miR-10a-5p upregulated the expression of ALP and RUNX2 *in vitro*. Furthermore, miR-10a-5p acted as a suppressor during the process of new bone formation *in vivo*. In conclusion, the findings of the present study suggested that miR-10a-5p served as a negative regulatory factor during osteoblast differentiation of hBMSCs and may be utilized in a treatment approach for bone repair in osteogenic-related diseases.

Introduction

Osteoporosis or bone fractures are major causes of general bone tissue loss, and currently, no specific treatment exists (1). With an aging population and the need for more efficacious therapeutics with fewer side effects, the field of bone tissue engineering is increasing (2,3). Stem cell therapies and tissue engineering applications are the most recent treatment options targeted to repair damaged organizational structures and restore physiological function of bone (4).

Human bone marrow mesenchymal stem cells (hBMSCs) are a type of multilineage stem cell that have the potential to differentiate into cells associated with mesenchymal tissues, including fat, cartilage, bone, tendon, marrow stroma and muscle (5). Over 10 years of research has focused on efforts to evaluate and utilize hBMSCs for tissue engineering and cell therapy applications, particularly in cardiovascular disorders, bone and cartilage regeneration, and neuronal damage, and through drip infusion or transplantation within scaffolds (6). Earlier research in the field of tissue-engineered bone regeneration employed mesenchymal stem cells collected from the human mandible or maxilla with substantial platelet-rich plasma. The results of those investigations revealed that bone tissue was regenerated with minimal invasiveness and good plasticity, and this could be used as a clinical alternative for autogenous bone transplantation (7,8).

MicroRNAs (miRNAs/miRs) are short non-coding RNAs that have a key role in regulating differentiation and self-renewal of stem cells (9). Almost all miRNAs bind to the 3' untranslated region of target mRNAs through an incomplete match that inhibits their translation and stability (10). The miR-10 family is highly conserved and has attracted the interest of several research groups due to its co-expression with the Hox gene development regulator and its regulation of nearby

Correspondence to: Dr Zedong Lan, Department of Orthodontics, Shenzhen Stomatological Hospital, Southern Medical University, 1092 Jianshe Road, Shenzhen, Guangdong 518001, P.R. China
E-mail: 1211872581@qq.com

*Contributed equally

genome localization (11,12). miR-10a has been demonstrated to regulate numerous pathways, including inflammation, cancer and proliferation processes (13-15). It has been reported that miR-204 and its homolog miR-211 act as negative regulators of osteoblast differentiation in BMSCs via the negative regulation of runt-related transcription factor 2 (RUNX2) transcription factors (16). A previous study has also found that miR-206 played an inhibitory role during osteoblast differentiation of MSCs (17). However, to the best of our knowledge, there is no information with regards to the specific modulatory effects of miR-10a-5p on osteogenic differentiation of hBMSCs.

Therefore, the aim of the present study was to investigate the relationship between hBMSCs and miR-10a-5p, and to determine how miR-10a-5p regulated the osteogenic differentiation process of hBMSCs *in vitro* and *in vivo*.

Materials and methods

Cell culture and osteogenic differentiation. hBMSCs (cat. no. HUXMA-01001; Cyagen Biosciences, Inc.) were cultured in OriCell™ human mesenchymal stem cell growth medium (cat. no. HUXMA-90011; Cyagen Biosciences, Inc.) containing 10% human mesenchymal stem cell-qualified fetal bovine serum (Cyagen Biosciences, Inc.), 1% penicillin-streptomycin and 1% glutamine at 37°C in 5% CO_2. The culture medium was changed every 3 days. Once the hBMSCs reached 80-90% confluence, they were dissociated with trypsin-EDTA and passaged. The cells were transferred into growth medium at a concentration of $2x10^5$ cells/cm^2 in 6-well tissue culture plates with a complete volume of 2 ml/well. Osteogenic differentiation was induced using OriCell mesenchymal stem cell osteogenic differentiation medium (cat. no. GUXMX-90021; Cyagen Biosciences, Inc.) containing 10% human mesenchymal stem cell-qualified fetal bovine serum, 1% penicillin-streptomycin, 1% glutamine, 0.2% ascorbate, 1% β-glycerophosphate and 0.01% dexamethasone.

RNA interference (RNAi) and miRNA mimics. mirVana™ miRNA hsa-miR-10a-5p inhibitor (cat. no. 4464084; Ambion; Thermo Fisher Scientific, Inc.) and mimic (cat. no. 4464066; Ambion; Thermo Fisher Scientific, Inc.) are small, chemically modified, single-stranded (ss) and double-stranded (ds) RNAs that inhibit and mimic endogenous miRNAs and enable miRNA functional analysis, through down- or upregulation of miRNA activity, respectively. The inhibitor negative control (inhibitor-negative; cat. no. 4464076) and mimic negative control (mimic-negative; cat. no. 4464058) were also purchased from Ambion (Thermo Fisher Scientific, Inc.). Adherent hBMSCs ($2x10^5$ cells/well) in 6-well tissue culture plates were treated with miRNA mimic, mimic-negative, inhibitor or inhibitor-negative diluted with RNase-free water at 25 nM as a final concentration. Diluted Lipofectamine® RNAi MAX Reagent (50 pmol) in 2 ml Opti-MEM® medium (Invitrogen; Thermo Fisher Scientific, Inc.) was added to each well and cells were incubated at 37°C in an atmosphere containing 5% CO_2 for 12 h. The medium was replaced with OriCell mesenchymal stem cell osteogenic differentiation medium for subsequent experiments immediately.

Fluorescent detection. BLOCK-iT™ Alexa Fluor® Red Fluorescent Control (Thermo Fisher Scientific, Inc.) is an Alexa Fluor® 555-labeled dsRNA duplex used for assessing lipid-mediated transfection for RNAi experiments. Cells seeded at 60-80% confluence were used for transfection, and Lipofectamine RNAiMAX (Invitrogen; Thermo Fisher Scientific, Inc.) was diluted in Opti-MEM. Alexa Fluor® 555-labeled dsRNA was diluted in Opti-MEM in a 5 ml Eppendorf tube®, and the diluted dsRNA (25 pmol) was added to the diluted Lipofectamine RNAiMAX reagent at a 1:1 ratio, and incubated for 5 min at room temperature. Then, the dsRNA-lipid complex was added to the hBMSCs for 24 h at 37°C. The nucleus was then stained using Hoechst 33342 working solution (cat. no. C1025; Beyotime Institute of Biotechnology) for 15 min at room temperature, rinsed with 0.01 mol/l phosphate-buffered saline (PBS) 3 times for 5 min each time. The transfection efficiency was visualized under an inverted fluorescence microscope (Leica Microsystems, Inc.). The time interval between transfection and visualization was 24 h.

Reverse transcription-quantitative PCR (RT-qPCR). For RT-qPCR analysis, total RNA was extracted from transfected hBMSCs with RNA Iso-Plus reagent (Takara Bio, Inc.). RT-qPCR was performed using the primers listed in Table I (Takara Bio, Inc.). The genomic DNA removal reaction was at 42°C for 2 min before storage at 4°C; RT was performed using the PrimeScript RT reagent kit with gDNA eraser (cat. no. DRR047A; Takara Bio, Inc.) in a 20-μl volume reaction system at 37°C for 15 min, followed by inactivation at 85°C for 5 sec storage at 4°C. The expression level differences were analyzed using Light Cycler® 480 SYBR Green I Master (Roche Diagnostics) in a 25-μl volume in accordance with the general manufacturer's protocol. PCR thermocycling was conducted as follows: Pre-denaturation at 95°C for 30 sec, followed by 40 cycles of denaturation at 95°C for 5 sec, primer annealing at 60°C for 30 sec and extension at 72°C for 1 min. The same RT-qPCR protocol was followed for miRNA detection, primers of human miR-10a-5p and internal control U6 were also purchased from Takara Bio, Inc. Amplification and detection were all performed using a 7500HT Fast Real-Time PCR system (Bio-Rad Laboratories, Inc.). Quantitative analysis was performed with the $2^{-\Delta\Delta Cq}$ method (18).

Cell viability assay. Cell Counting Kit-8 (CCK-8; Dojindo Molecular Technologies, Inc.) was used to measure the effects of RNAi on hBMSC viability. Transfected and non-transfected cells were plated at a concentration of $2x10^5$ cells/well in 6-well plates with 2 ml complete medium for 12 h. The blank group was 2 ml complete medium without cells. CCK-8 reagent was added (10 μl/well), and all groups were incubated at 37°C in 5% CO_2 for 4 h. Cell viability was measured at an optical density (OD) of 450 nm. Cell viability (%) = [OD (transfected cells)-OD (blank)]/[OD (non-transfected cells)-OD (blank)] x100%.

Adipogenic differentiation analysis. Adipogenic differentiation of transfected hBMSCs was induced using mesenchymal stem cell adipogenic differentiation medium (cat. no. GUXMX-90031; Cyagen Biosciences, Inc.) containing 10% human mesenchymal stem cell-qualified fetal bovine

Table I. Primers used for reverse transcription-quantitative PCR.

Gene	Primer sequence (5'→3')
GAPDH	F: GCACCGTCAAGGCTGAGAAC
	R: TGGTGAAGACGCCAGTGGA
ALP	F: GCTCATGCATAACATCAGGGACA
	R:TCGTCACTCTCATACTCCACATCAG
RUNX2	F: CACTGGCGCTGCAACAAGA
	R: CATTCCGGAGCTCAGCAGAATAA
U6	F:GCTTCGGCAGCACATATACTAAAAT
	R: CGCTTCACGAATTTGCGTGTCAT

F, forward; R, reverse; ALP, alkaline phosphatase; miR, microRNA; RUNX2, runt-related transcription factor 2.

serum, 1% penicillin-streptomycin, 0.2% insulin, 0.1% IBMX, 0.1% rosiglitazone and 0.1% dexamethasone for 7 days. Following cell differentiation, the adipogenic differentiation medium was removed from the wells and cells were rinsed with 1X PBS. Cells were then fixed with 2 ml of 4% formaldehyde solution for 30 min at room temperature. Wells were rinsed twice with 1X PBS and cells were stained with 1 ml oil red O (Cyagen Biosciences, Inc.) working solution (3:2 dilution with distilled water; filtered) for 30 min at room temperature. Finally, cells were rinsed 2-3 times with 1X PBS, and were visualized and analyzed under a light microscope.

Western blot analysis. Transfected hBMSCs were lysed with radio immunoprecipitation buffer (Beyotime Institute of Biotechnology) and a Bradford kit (Beyotime Institute of Biotechnology) was used to determine total protein concentration. Proteins (20 μg/lane) were isolated by SDS-PAGE on 10% gels and were electrotransferred onto nitrocellulose membranes (cat. no. IPVH00010; EMD Millipore); membranes were then blocked with 1% BSA (Beyotime Institute of Biotechnology) to ensure non-specific binding for 60 min at room temperature. Membranes were incubated with anti-rabbit alkaline phosphatase (ALP; 1:1,000; cat. no. ab75699; Abcam), anti-rabbit RUNX2 (1:1,000; cat. no. ab192256; Abcam) and anti-rabbit GAPDH (1:20,000; cat. no. ab181602; Abcam) primary antibodies at 4°C overnight. Anti-HRP (1:2,000; cat. no. ab181658; Abcam) secondary antibody was used to incubate the membrane for 1 h at room temperature. All antibodies were diluted with dH$_2$O (Takara Bio, Inc.). Protein bands were observed by enhanced chemiluminescence (Beyotime Institute of Biotechnology) and exposed on X-ray film (Kodak). The relative grey values were analyzed by ImageJ 1.48 software (National Institutes of Health).

Animal model construction. The present study was reviewed and approved as appropriate and humane by the Institutional Animal Care and Use Committee of Guangzhou Medical University (Guangzhou, China). All research was performed in accordance with the regulations as outlined by the National Institutes of Health (19). Animals were anesthetized before incision and sacrificed in accordance with the council

directive of the European Community of 24 November 1986 (86/609/EEC), the Care and Use of Animal Testing Procedures, and local laws and regulations. A total of 4-week-old, female BALB/c mice (weight, ~20 g) supplied by Guangdong Medical Laboratory Center (Guangzhou, China) were separated into six groups (blank, control, mimic, mimic-negative, inhibitor and inhibitor-negative). The mice were raised in a sterile environment with a relative humidity of 40-70% at a temperature of 20-26°C, in a light/dark cycle of 12/12 h. The average feed consumption per 100 g body weight was 5 g, and the water consumption was 7 ml. Transfected and non-transfected (control group) hBMSCs were loaded onto 10x8x2 mm^3 hydroxyapatite/tricalcium-phosphate (HA/TCP) cubic scaffolds with porosity of 30% (Department of Inorganic Material, Sichuan University, Chengdu, China) at a ratio of 1:3 and the loaded scaffolds were then subcutaneously implanted into the BALB/c mice. The blank group was transplanted with HA/TCP scaffolds only (without hBMSCs). Two longitudinal skin incisions ~1.5 cm in length were made on the dorsal surface of each mouse and subcutaneous pouches were made using vascular forceps. One HA/TCP implant with cells was implanted in each pouch (two in each mouse). Surgical sutures were used to close the incisions and the mice were placed in separate cages until the end of the experiment. The aforementioned step was repeated on each mouse in the study. The graft was maintained *in vivo* for 4 weeks.

Preparation of specimens for scanning electron microscopy (SEM). The scaffolds with transfected hBMSCs and the non-cellular scaffolds were cultured for 12 h and fixed immediately at 1% glutaraldehyde for 12 h at 4°C. The specimens were then rinsed twice with PBS, post-fixed in 1% osmium tetroxide for 1 h at room temperature, subsequently rinsed twice in PBS and dehydrated in a graded series of alcohol (40, 70, 90 and 100%) for 10 min each and allowed to dry. The silver membrane (1,500 nm thick) was layered on the scaffold surface and prepared for SEM at 10 kV.

Goldner's trichrome staining. After an 8-week transplantation period, the mice were sacrificed by cervical dislocation. The implants were removed and fixed with 4% paraformaldehyde at 4°C for 24 h. According to the manufacturer's instructions, a plastic block with a mineralized implant was obtained for sectioning using the Technovit 9100 methyl methacrylate kit (Electron Microscopy Sciences). Using a heavy-duty microtome (E300CP; EXAKT Advanced Technologies GmbH), three serial sections (5 μm) were taken close to the surface of the block and slices were repeated each 100 μm to obtain a total of nine levels of implantation, by implantation depth. The Goldner's trichrome staining (Electron Microscopy Sciences) was used for histological analysis of heterogeneous new bone formation under light microscopy, following the recommended protocol (20).

Micro-CT analysis of the implants. The implants were scanned with Skycan® Micro-CT (Bruker Corporation) at 65 kV, 80 μA with an isotropic resolution of 12 μm of three spatial dimensions, using CTAn v1.18 (Bruker Corporation) analysis for each experimental group. Bone volume (BV) was calculated using the closed volume triangular surface corresponding to
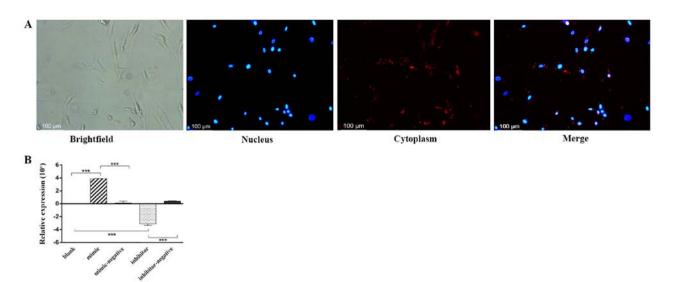
Figure 1. Transfection efficiency. (A) RNAs appeared in the nucleus, which was evidenced by red staining, the nucleus was stained blue with Hoechst stain, (magnification, x10). (B) Compared with the blank group (set at 0), the miR-10a-5p mimic group had significantly higher miR-10a-5p levels, whereas the miR-10a-5p inhibitor group had significantly lower miR-10a-5p levels. ***P<0.001. miR, microRNA.

the tetrahedron. Total bone volume was the volume of the entire sample being examined.

Statistical analysis. Statistical analysis was performed using SPSS 16.0 (SPSS, Inc.). Experiments were repeated three times and data are presented as mean ± standard deviation. Comparisons for experiments with >2 subgroups were analyzed by one-way ANOVA followed by Tukey's post hoc test. P<0.05 was considered to indicate a statistically significant difference.

Results

Transfection efficiency. After 24 h of transfection, Alexa Fluor® 555-labeled, dsRNAs appeared in the cytoplasm as a red fluorescence signal surrounding the nucleus (blue) under an inverted fluorescence microscope (Fig. 1A). The relative expression levels of miR-10a-5p were analyzed by RT-qPCR in the different experimental groups. Compared with the blank group (classed as 0) and the mimic-negative group, miR-10a-5p expression in the mimic group was significantly higher. Whereas, the miR-10a-5p inhibitor group exhibited significantly lower levels of miR-10a-5p than the blank and the inhibitor-negative group (P<0.001; Fig. 1B).

Cell viability. Additionally, 24 h post-transfection hBMSCs, cultured in the OriCell human mesenchymal stem cell growth medium with 10 μl CCK-8 reagent, were used to assess cell viability. The OD values demonstrated no significant difference among the groups studied and the average percentage of cell viability reached 79%. Lipofectamine, miR-10a-5p mimics and inhibitors had no influence on cell viability (Fig. 2).

Osteoblast differentiation of hBMSCs in vitro. mRNA expression levels of mineralization-related genes were measured during osteoblast differentiation by RT-qPCR at 7, 14 and 21 days post-transfection (Fig. 3A). At all three time points, the relative expression of ALP in the mimic group was ~1-fold lower than the blank group (P<0.05). The inhibitor group

exhibited a higher expression level of ALP compared with the blank group (P<0.05). The changes in the relative expression of RUNX2 in the various groups were even more significant (P<0.01). The results indicated that miR-10a-5p had a negative regulatory effect on the osteogenic processes of hBMSCs (P<0.05). To further investigate the effects of miR-10a-5p on post-transcription expression, the protein expression levels of ALP and RUNX2 were evaluated in the experimental groups using western blotting 14 days post-transfection (Fig. 3B). Compared with the blank group, the protein levels of RUNX2 and ALP were significantly decreased in the mimic group, whereas the levels were significantly increased in the inhibitor group (P<0.05) (Fig. 3B and C). No significant differences were found among the blank, mimic-negative and inhibitor-negative groups. The protein expression of RUNX2 and ALP confirmed that miR-10a-5p was a potential negative regulator of osteoblast differentiation *in vitro*.

Adipogenic differentiation of hBMSCs in vitro. Oil red O staining of transfected hBMSCs was performed 7 days after induction in the blank (Fig. 4A), mimic (Fig. 4B) and inhibitor (Fig. 4C) groups. Compared with the blank group, the number of lipid droplets in the miR-10a-5p group was increased, whereas the number of lipid droplets in the inhibitor group was reduced. Therefore, it was hypothesized that miR-10a-5p may have a positive regulatory role in hBMSCs adipogenic differentiations.

Culturing hBMSCs in the scaffold. To explore whether the regulation of miR-10a-5p expression in hBMSCs influenced bone formation *in vivo*, the transfected hBMSCs were transferred into scaffolds and cultured for 4 days. In an effort to promote ectopic bone formation, hBMSCs were loaded into the HA/TCP scaffolds, incubated for 24 h and subcutaneously implanted in BALB/c mice. The hBMSCs morphology and attachment to the porous surface of the HA/TCP scaffold (Fig. 5A), in comparison with non-cellular scaffolds used as a control group, was observed using SEM (Fig. 5B). hBMSCs
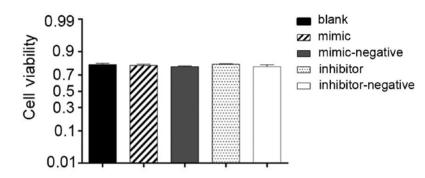
Figure 2. Cell viability. The optical density values showed no significant difference among the groups. Based on this evidence, Lipofectamine and the miR-10a-5p mimic and inhibitor groups were assumed to have had no effect on cell viability. miR, microRNA.

adhered to the surface of the scaffold and extended their pseudopodia confirming a conducive environment for growth conditions (Fig. 5C and D).

miR-10a-5p suppresses ectopic bone formation in vivo. Specimens stained with Goldner's trichrome illustrated different stages of bone mineralization under the microscope. Fig. 6A displays a general overview of histological sections. Bone and bone-like tissues are presented as a substructure visualized in green and light purple and the HA/TCP scaffold was presented as a dark green positive control. The connective tissue is displayed as a structural network of cells and collagen fibers in orange and pink (Fig. 6A-F). Inside the pores of the scaffold, less new bone formation was noted in the scaffold-only groups in comparison with the scaffolds containing cells. The mineralization area seen with the blank group was only slightly more than that seen in the negative controls. As hypothesized, the inhibitor group produced more new bone tissues than the blank group. Conversely, the mimic-only group had small and barely visible purple staining, which confirmed limited amounts of early stage bone formation (Fig. 6G-L). These results suggested that miR-10a-5p also had a negative regulation *in vivo*. Regular breeding mice were sacrificed at 8 weeks and the scaffold transplants were collected with some margins of soft tissue. The bone volume values of the samples were 101.9 ± 3.16 (control), 113.4 ± 3.38 (blank), 107.9 ± 3.21 (mimic), 103.8 ± 8.40 (mimic-negative), 108.3 ± 3.54 (inhibitor) and 104.4 ± 1.84 mm^3 (inhibitor-negative) ($P>0.05$) with no significant difference noted among the groups. Therefore, with the volume of the scaffolds ~equal, this would not have an overall effect on the final results (Fig. 6M).

Discussion

hBMSCs have a great potential for differentiation into multiple lineages and serve as the ideal source for remodeling bone tissue to recover body functions. Their clinical potential for gene-based therapy applications is rapidly being recognized (21,22). Several miRNAs are currently being studied for their involvement in the inhibition of osteoblast differentiation and may become important for regulating bone remodeling. The present study explored the role and regulation of miR-10a-5p in osteogenesis, including *in vitro* and *in vivo* experiments. The influence of miR-10a-5p on the adipogenic process was also investigated.

RNAi, a conserved evolutionary mechanism widely found in nature, can induce gene silencing by prohibiting the translation of the target Mrna (23). RNAi affects the post-transcriptional expression levels of several genes. miRNAs pair with mRNA regions and target them for degradation (24). The first step in this process is ensuring the RNA can base pair with a region of its target gene; once base pairing is completed, the target proteins, including drosha, dicer and argonaute, direct the mRNA to nuclease destruction (25). miRNA mimics are small, chemically modified dsRNAs, which mimic endogenous miRNAs and make functional analysis of miRNAs possible by upregulating miRNA activity. miRNA inhibitors are small, chemically modified ssRNA molecules that specifically bind and inhibit endogenous miRNA molecules, thereby enabling functional analysis of miRNAs by downregulating miRNA activity. Both are recommended for *in vivo* and *in vitro* applications.

In the present study, the role of miR-10a-5p in the process of bone formation *in vitro* was studied to provide evidence for bone formation *in vivo*. Two classic target genes are associated with bone formation in the transcriptional and post-transcriptional stages. RUNX2 belongs to the runt-associated transcription factor family (26) and is closely associated with the osteoblast phenotype. The human RUNX2 gene has been identified and located on chromosome 6p21. RUNX2, also known as Cbfa1, is an early major transcription factor that initiates the process of osteoblastic lineage transcription (27,28). Izu *et al* (29) demonstrated that the expression of RUNX2 was increased in early-stage osteoblast development when compared with wild type cells. Several studies regarding miRNAs that regulate RUNX2 expression have used MC3T3-E1 and ATDC5 cells, which originate from human mesenchymal stem cells (30,31). A previous study noted that miR-30c, miR-133a, miR-135 and miR-338 strongly inhibited RUNX2 protein expression (32). Another study confirmed that C-X-C motif chemokine ligand 13 mediated upregulation of RUNX2 by inhibiting miR-23a (33). These studies all support the results from the present study, which indicated that RUNX2 expression was inhibited by miR-10a-5p. However, overexpression of RUNX2 induced the transcription of miR-10a/10b in breast cancer cell lines, and also impaired cell motility. Whereas, inhibition of RUNX2 decreased miR-10a/10b expression and impaired cell migration and invasion ability (34). ALP is a type of extracellular membrane protein that is downregulated during bone formation (35). A previous study on miR-214 suggested that
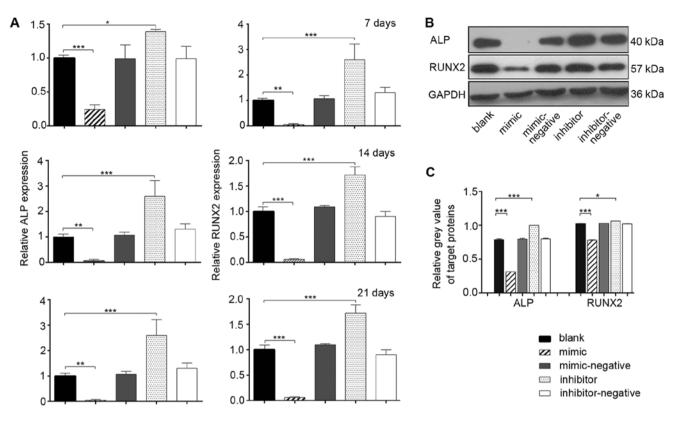
Figure 3. Osteoblast differentiation of human bone marrow mesenchymal stem cells *in vitro*. (A) mRNA expression levels of ALP and RUNX2 were measured using reverse transcription-quantitative PCR at 7, 14 and 21 days post-transfection. (B and C) Protein expression levels of ALP and RUNX2 in different groups were studied with western blotting at 14 days post-transfection. *P<0.05, **P<0.01, ***P<0.001. ALP, alkaline phosphatase; miR, microRNA; RUNX2, runt-related transcription factor 2.
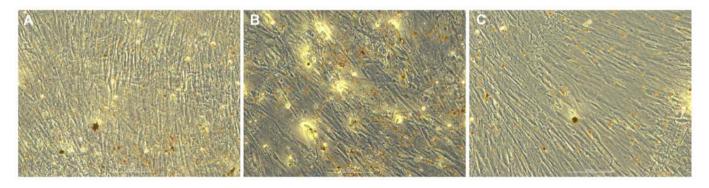

Figure 4. Oil red O staining of transfected human bone marrow mesenchymal stem cells. Staining was performed 7 days post-transfection in the (A) blank, (B) miR-10a-5p mimic and (C) miR-10a-5p inhibitor groups. Scale bar, 200 μm. miR, microRNA.

ALP mRNA expression levels were continuously decreased in MC3T3-E1 cells for 33 days, starting from day 6 with an interval of 3 days (36), and the trend observed in the present study produced similar results. Conversely, overexpression of miR-210 promoted the osteoblast differentiation of hBMSCs via the PI3K/AKT pathway by increasing the expression of ALP and osterix (37). miRNAs modulate their target genes through different signaling pathways, which might have opposite outcomes (38-40). RUNX2 has been reported to directly regulate the transcription of target genes, including ALP and osteocalcin (41). This suggests why the high expression of RUNX2 is easily found, whereas there is a slight discrepancy in the role of ALP expression in the late stage of osteogenesis.

Only a few studies have examined the role of miRNAs in bone formation or osteoblast phenotypic development *in vivo* (42-45). However, the present study performed an *in vivo* investigation and confirmed that new bone formation resulted from hBMSCs and not host mouse cells. The chemical composition and crystal structure of HA are very similar to those of natural bone tissue, and it has valuable biocompatibility and osteoinductive effects. However, the absorption of HA is very low (46). In contrast, TCP is an absorbable, biocompatible bone substitute with improved degradability and bone regeneration ability compared with HA. Since the degradation of HA and TCP are complementary, specific proportions must be used in order for the bone substitute material to have the
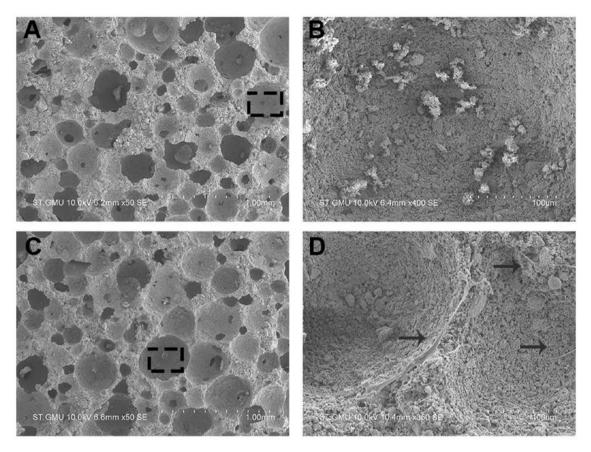
Figure 5. Culturing hBMSCs in the scaffold. (A) Under SEM, the morphology of the porous surface of HA/TCP was observed using magnification x50, and (B) magnification x400. (C) Morphology of hBMSCs on the HA/TCP scaffold using magnification x50 and (D) magnification x350, hBMSCs (arrow) adhered to the surface of the scaffold and extended their pseudopodium as seen under SEM, suggesting suitable topographic conditions for cellular attachment and growth. HA/TCP, hydroxyapatite/tricalcium-phosphate; hBMSCs, human bone marrow mesenchymal stem cells; SEM, scanning electron microscopy.

ideal properties (optimized dissolution and resorption) for the bone remodeling process to be effective (47). The combination of HA and TCP can improve bone regeneration and extend the medical applications of these artificial materials (48). It has previously been shown that bidirectional calcium phosphate created by mixing HA and TCP at a ratio of 1:3 had improved absorbability than that observed with TCP alone (49).

BALB/c mice lack a thymus, leading to a deficiency in cellular immunity; however, their humoral immunity is normal. In this way, rejection and inflammatory reactions are not seen as serious following surgery, thereby creating a more stable microenvironment, which is beneficial to transfected hBMSCs proliferation and differentiation. By choice, the hard tissue slicing embedment did not require decalcification of the samples. Therefore, the present study avoided the normal mineralized tissue being damaged by acid or EDTA, and more clearly observed the difference between experimental and control groups. Goldner's trichrome staining contains Weigert's iron hematoxylin, ponceau acid fuchsin, phosphomolybdic acid-orange G and light green solutions. This staining procedure is a commonly used method in bone histology and allows for tissue identification by colorimetric and morphological differences. In addition, the staining can also allow for a clear separation of connective tissue and bone matrix (50). The results of the present study indicated that miR-10a-5p downregulated bone formation post-transfection. It has previously been reported that miR-206, miR-124 and

miR-138 inhibited osteoblastogenesis *in vivo*, by targeting different signal molecules (17,51,52). In order to apply these findings to the clinic, further studies are required to elucidate the mechanism involved.

In the present study, the specific mechanism by which miR-10a-5p affects the expression of RUNX2 and ALP, and ultimately affects the process of osteogenic differentiation was not studied in detail. Liu *et al* (53) demonstrated that inhibiting the expression of miR-29b, upregulating DNA methyltransferase 1 and downregulating Notch1 and Notch intracellular domain, ultimately upregulated the expression of RUNX2 and ALP via the Notch signaling pathway. In high-fat diet-fed mice, the Notch1 expression levels were increased when compared with normal diet-fed mice, whereas the expression levels of RUNX2 and ALP were relatively low in the high-fat diet group (54). Zou *et al* (55) also reported that a forward genetic screen yielded the microtubule-associated protein, DCAMKL1, which suppressed osteoblast activation by antagonizing RUNX2. DCAMKL1 is associated with several miRNAs, including miR-200a, let-7a and miR-144, in different types of tissue (56-58). Notably, marrow adipocytes have been reported to exhibit osteogenic and adipogenic characteristics, and are particularly responsive to parathyroid hormone (PTH) and secrete receptor activator of nuclear factor-κB ligand (RANKL) (59). IL-17A may also mediate the bone catabolic activity of continuous PTH by upregulating the production of RANKL to induce bone loss via Gαs/cAMP/Ca^{2+}
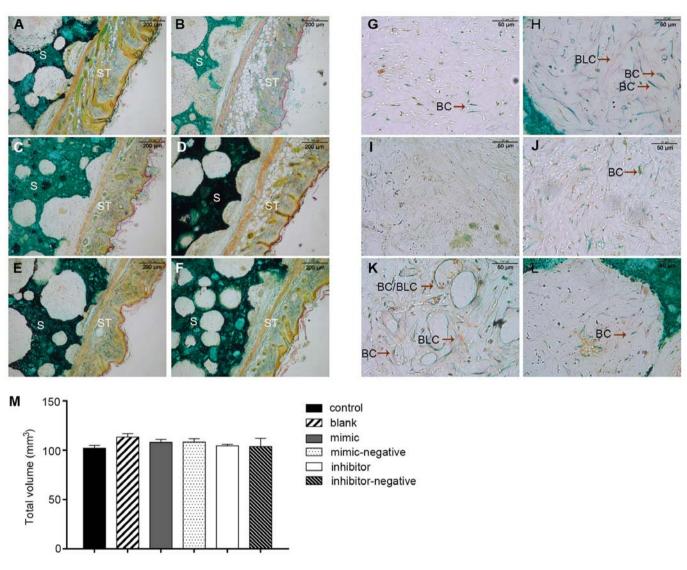
Figure 6. Two transplants per treatment were engrafted into mice and three sections of each transplant were stained and investigated. Images from (A) control, (B) blank, (C) mimic, (D) mimic-negative, (E) inhibitor and (F) inhibitor-negative group. Embedded S and ST were stained with Goldner's trichrome. The cuticular, dermal, subcutaneous tissue and HA/TCP were easily observed (magnification, x10). (G-L) Inside the pores of scaffolds, BC were green and BLC were purple (magnification, x40). The scaffold transplants from mice were collected with some margins of soft tissue. (M) Bone volume values of samples were 101.9±3.16, 113.4±3.38, 107.9±3.21, 103.8±8.40, 108.3±8.4 and 104.4±1.84 mm^3 in the groups, with no significant difference noted among the groups. BC, bone cells; BLC, bone-like cells; HA/TCP, hydroxyapatite/tricalcium-phosphate; S, scaffolds; ST, soft tissues.

signaling (60). Therefore, there remains much work to be performed in order to understand the mechanism underlying miR-10a-5p-regulated osteogenesis.

In conclusion, miR-10a-5p could be utilized as a negative regulator of osteoblastic differentiation of hBMSCs and may have a positive effect on adipogenesis. Notably, the results of the present study demonstrated that the functional inhibition of miR-10a-5p expedited osteogenic differentiation of hBMSCs and led to promotion of bone formation *in vivo*. Furthermore, the present study suggested that use of miR-10a-5p-targeting treatments could promote bone formation, and ultimately may be used for the treatment of pathological bone loss, cardiovascular disorders, bone and cartilage regeneration, and neuronal damage.

Acknowledgements

Not applicable.

Availability of data and materials

The datasets used and/or analyzed during the current study are available from the corresponding author on reasonable request.

Authors' contributions

YZ and ZL conceived and designed the experiments. LZ, ZZ, FR and LC performed the experiments. YZ, LZ and ZL analyzed the data and wrote the manuscript. All authors read and approved the final manuscript.

Ethics approval and consent to participate

The present study was reviewed and approved as appropriate and humane by the Institutional Animal Care and Use Committee of Guangzhou Medical University. All research was performed in accordance with the regulations as outlined by the National Institutes of Health. Animals were anesthetized and sacrificed in accordance with the council directive of the European Community of 24 November 1986 (86/609/EEC), the Care and Use of Animal Testing Procedures and local laws and regulations.

Patient consent for publication

Not applicable.

Competing interests

The authors declare that they have no competing interests.

References

1. Pichler K, Loreto C, Leonardi R, Reuber T, Weinberg AM and Musumeci G: Rankl is downregulated in bone cells by physical activity (treadmill and vibration stimulation training) in rat with glucocorticoid-induced osteoporosis. Histol Histopathol 28: 1185-1196, 2013.
2. Castrogiovanni P, Trovato FM, Szychlinska MA, Nsir H, Imbesi R and Musumeci G: The importance of physical activity in osteoporosis. From the molecular pathways to the clinical evidence. Histol Histopathol 31: 1183-1194, 2016.
3. Cardinale M and Bosco C: The use of vibration as an exercise intervention. Exerc Sport Sci Rev 31: 3-7, 2003.
4. Srinivasaiah S, Musumeci G, Mohan T, Castrogiovanni P, Absenger-Novak M, Zefferer U, Mostofi S, Bonyadi Rad E, Grün NG, Weinberg AM and Schäfer U: A 300 μm organotypic bone slice culture model for temporal investigation of endochondral osteogenesis. Tissue Eng Part C Methods 25: 197-212, 2019.
5. Pittenger MF, Mackay AM, Beck SC, Jaiswal RK, Douglas R, Mosca JD, Moorman MA, Simonetti DW, Craig S and Marshak DR: Multilineage potential of adult human mesenchymal stem cells. Science 284: 143-147, 1999.
6. Szychlinska MA, Castrogiovanni P, Nsir H, Di Rosa MD, Guglielmino C, Parenti R, Calabrese G, Pricoco E, Salvatorelli L, Magro G, et al: Engineered cartilage regeneration from adipose tissue derived-mesenchymal stem cells: A morphomolecular study on osteoblast, chondrocyte and apoptosis evaluation. Exp Cell Res 357: 222-235, 2017.
7. Yamada Y, Ueda M, Hibi H and Nagasaka T: Translational research for injectable tissue-engineered bone regeneration using mesenchymal stem cells and platelet-rich plasma: From basic research to clinical case study. Cell Transplant 13: 343-355, 2004.
8. Yamada Y, Nakamura S, Ito K, Kohgo T, Hibi H, Nagasaka T and Ueda M: Injectable tissue-engineered bone using autogenous bone marrow-derived stromal cells for maxillary sinus augmentation: Clinical application report from a 2-6-year follow-up. Tissue Eng Part A 14: 1699-1707, 2008.
9. Lau NC, Lim LP, Weinstein EG and Bartel DP: An abundant class of tiny RNAs with probable regulatory roles in Caenorhabditis elegans. Science 294: 858-862, 2001.
10. Rana TM: Illuminating the silence: Understanding the structure and function of small RNAs. Nat Rev Mol Cell Biol 8: 23-36, 2007.
11. Tanzer A, Amemiya CT, Kim CB and Stadler PF: Evolution of microRNAs located within hox gene clusters. J Exp Zool B Mol Dev Evol 304: 75-85, 2005.
12. Woltering JM and Durston AJ: Mir-10 represses hoxb1a and hoxb3a in zebrafish. PLoS One 3: e1396, 2008.
13. Mu N, Gu J, Huang T, Zhang C, Shu Z, Li M, Hao Q, Li W, Zhang W, Zhao J, et al: A novel NF-κB/YY1/MicroRNA-10a regulatory circuit in fibroblast-like synoviocytes regulates inflammation in rheumatoid arthritis. Sci Rep 6: 20059, 2016.
14. Liang D, Zhen L, Yuan T, Huang J, Deng F, Wuyahan, Zhang H, Pan L, Liu Y, The E, et al: miR-10a regulates proliferation of human cardiomyocyte progenitor cells by targeting GATA6. PLoS One 9: e103097, 2014.
15. Xiong G, Huang H, Feng M, Yang G, Zheng S, You L, Zheng L, Hu Y, Zhang T and Zhao Y: miR-10a-5p targets TFAP2C to promote gemcitabine resistance in pancreatic ductal adenocarcinoma. J Exp Clin Cancer Res 37: 76, 2018.
16. Huang J, Zhao L, Xing L and Chen D: MicroRNA-204 regulates Runx2 protein expression and mesenchymal progenitor cell differentiation. Stem Cells 28: 357-364, 2010.
17. Inose H, Ochi H, Kimura A, Fujita K, Xu R, Sato S, Iwasaki M, Sunamura S, Takeuchi Y, Fukumoto S, et al: A microRNA regulatory mechanism of osteoblast differentiation. Proc Natl Acad Sci USA 106: 20794-20799, 2009.
18. Livak KJ and Schmittgen TD: Analysis of relative gene expression data using real-time quantitative pcr and the 2(-Delta Delta C(T)) method. Methods 25: 402-408, 2001.
19. National Research Council: Guide for the Care and Use of Laboratory Animals: Eighth Edition. The National Academies Press, Washington, DC, 2011.
20. Kanczler JM, Ginty PJ, Barry JJ, Clarke NM, Howdle SM, Shakesheff KM and Oreffo RO: The effect of mesenchymal populations and vascular endothelial growth factor delivered from biodegradable polymer scaffolds on bone formation. Biomaterials 29: 1892-1900, 2008.
21. Reiser J, Zhang XY, Hemenway CS, Mondal D, Pradhan L and La Russa VF: Potential of mesenchymal stem cells in gene therapy approaches for inherited and acquired diseases. Expert Opin Biol Ther 5: 1571-1584, 2005.
22. Chen L, Xu Y, Zhao J, Zhang Z, Yang R, Xie J, Liu X and Qi S: Conditioned medium from hypoxic bone marrow-derived mesenchymal stem cells enhances wound healing in mice. PLoS One 9: e96161, 2014.
23. Bernstein E, Caudy AA, Hammond SM and Hannon GJ: Role for a bidentateribonuclease in the initiation step of RNA interference. Nature 409: 363-366, 2001.
24. Fire A, Xu S, Montgomery MK, Kostas SA, Driver SE and Mello CC: Potent and specific genetic interference by double-stranded RNA in Caenorhabditis elegans. Nature 391: 806-811, 1998.
25. Morris KV and Mattick JS: The rise of regulatory RNA. Nat Rev Genet 15: 423-437, 2014.
26. Van Wijnen AJ, Stein GS, Gergen JP, Groner Y, Hiebert SW, Ito Y, Liu P, Neil JC, Ohki M and Speck N: Nomenclature for Runt-related (RUNX) proteins. Oncogene 23: 4209-4210, 2004.
27. Rosen CJ: Bone remodeling, energy metabolism, and the molecular clock. Cell Metab 7: 7-10, 2008.
28. Musumeci G, Mobasheri A, Trovato FM, Szychlinska MA, Graziano AC, Lo Furno D, Avola R, Mangano S, Giuffrida R and Cardile V: Biosynthesis of collagen I, II, RUNX2 and lubricin at different time points of chondrogenic differentiation in a 3D in vitro model of human mesenchymal stem cells derived from adipose tissue. Acta Histochem 116: 1407-1417, 2014.
29. Izu Y, Sun M, Zwolanek D, Veit G, Williams V, Cha B, Jepsen KJ, Koch M and Birk DE: Type XII collagen regulates osteoblast polarity and communication during bone formation. J Cell Biol 193: 1115-1130, 2011.
30. Liu Y, Xu F, Pei HX, Zhu X, Lin X, Song CY, Liang QH, Liao EY and Yuan LQ: Vaspin regulates the osteogenic differentiation of MC3T3-E1 through the Pi3K-Akt/miR-34c loop. Sci Rep 6: 25578, 2016.
31. Bonyadi Rad E, Musumeci G, Pichler K, Heidary M, Szychlinska MA, Castrogiovanni P, Marth E, Böhm C, Srinivasaiah S, Krönke G, et al: Runx2 mediated induction of novel targets ST2 and Runx3 leads to cooperative regulation of hypertrophic differentiation in ATDC5 chondrocytes. Sci Rep 7: 17947, 2017.
32. Zhang Y, Xie RL, Croce CM, Stein JL, Lian JB, Van Wijnen AJ and Stein GS: A program of microRNAs controls osteogenic lineage progression by targeting transcription factor Runx2. Proc Natl Acad Sci USA 108: 9863-9868, 2011.

33. Tian F, Ji XL, Xiao WA, Wang B and Wang F: CXCL13 promotes osteogenic differentiation of mesenchymal stem cells by inhibiting miR-23a expression. Stem Cells Int 2015: 632305, 2015.

34. Chang CH, Fan TC, Yu JC, Liao GS, Lin YC, Shih AC, Li WH and Yu AL: The prognostic significance of RUNX2 and miR-10a/10b and their inter-relationship in breast cancer. J Transl Med 12: 257, 2014.

35. Saltiel AR: Structural and functional roles of glycosylphosphoinosites. Subcell Biochem 26: 65-185, 1996.

36. Wang X, Guo B, Li Q, Peng J, Yang Z, Wang A, Li D, Hou Z, Lv K, Kan G, *et al*: miR-214 targets ATF4 to inhibit bone formation. Nat Med 19: 93-100, 2013.

37. Liu XD, Cai F, Liu L, Zhang Y and Yang AL: MicroRNA-210 is involved in the regulation of postmenopausal osteoporosis through promotion of VEGF expression and osteoblast differentiation. Biol Chem 396: 339-347, 2015.

38. Shen E, Diao X, Wei C, Wu Z, Zhang L and Hu B: MicroRNAs target gene and signaling pathway by bioinformatics analysis in the cardiac hypertrophy. Biochem Biophys Res Commun 397: 380-385, 2010.

39. Cao Q, Li YY, He WF, Zhang ZZ, Zhou Q, Liu X, Shen Y and Huang TT: Interplay between microRNAs and the STAT3 signaling pathway in human cancers. Physiol Genomics 45: 1206-1214, 2013.

40. Zhang W, Xie Y, Xu L, Wang Y, Zhu X, Wang R, Zhang Y, Muleke EM and Liu L: Identification of microRNAs and their target genes explores miRNA-mediated regulatory network of cytoplasmic male sterility occurrence during anther development in radish (Raphanus sativus L.). Front Plant Sci 7: 1054, 2016.

41. Otto F, Lübbert M and Stock M: Upstream and downstream targets of RUNX proteins. J Cell Biochem 89: 9-18, 2003.

42. Park J, Wada S, Ushida T and Akimoto T: The microRNA-23a has limited roles in bone formation and homeostasis in vivo. Physiol Res 64: 711-719, 2015.

43. Taipaleenmä H, Eskildsen T, Stenvang J, Abdallah MB, Ditzel N, Säämäne AM, Kauppine S and Kasse M: Mir-138 is a novel regulator of in vivo bone formation. Bone 47 (Suppl 1): S46, 2010.

44. Chen L, Holmstrøm K, Qiu W, Ditzel N, Shi K, Hokland L and Kassem M: MicroRNA-34a inhibits osteoblast differentiation and in vivo bone formation of human stromal stem cells. Stem Cells 32: 902-912, 2014.

45. Liu L, Liu M, Li R, Liu H, Du L, Chen H, Zhang Y, Zhang S and Liu D: MicroRNA-503-5p inhibits stretch-induced osteogenic differentiation and bone formation. Cell Biol Int 41: 112-123, 2017.

46. Hattori S: Structural features of ectopic bone-like tissue in porous hydroxyapatite blocks. Kokubyo Gakkai Zasshi 75: 120-137, 2008 (In Japanese).

47. Mayr H, Schlüfter S, Detsch R and Ziegler G: Influence of phase composition on degradation and resorption of biphasic calcium phosphate ceramics. Key Eng Mater 361-363: 1043-1046, 2008.

48. Daculsi G, Laboux O, Malard O and Weiss P: Current state of the art of biphasic calcium phosphate bioceramics. J Mater Sci Mater Med 14: 195-200, 2003.

49. Yamada S, Heymann D, Bouler JM and Daculsi G: Osteoclasticresorption of calcium phosphate ceramics with different hydroxyapatite/beta-tricalcium phosphate ratios. Biomaterials 18: 1037-1041, 1997.

50. Rentsch C, Schneiders W, Manthey S, Rentsch B and Rammelt S: Comprehensive histological evaluation of bone implants. Biomatter 4: e27993, 2014.

51. Eskildsen T, Taipaleenmäki H, Stenvang J, Abdallah BM, Ditzel N, Nossent AY, Bak M, Kauppinen S and Kassem M: MicroRNA-138 regulates osteogenic differentiation of human stromal (mesenchymal) stem cells in vivo. Proc Natl Acad Sci USA 108: 6139-6144, 2011.

52. Qadir AS, Um S, Lee H, Baek K, Seo BM, Lee G, Kim GS, Woo KM, Ryoo HM and Baek JH: miR-124 negatively regulates osteogenic differentiation and in vivo bone formation of mesenchymal stem cells. J Cell Biochem 116: 730-742, 2015.

53. Liu S, Liu D, Chen C, Hamamura K, Moshaverinia A, Yang R, Liu Y, Jin Y and Shi S: MSC transplantation improves osteopenia via epigenetic regulation of notch signaling in lupus. Cell Metab 22: 606-618, 2015.

54. Luo Y, Chen GL, Hannemann N, Ipseiz N, Krönke G, Bäuerle T, Munos L, Wirtz S, Schett G and Bozec A: Microbiota from obese mice regulate hematopoietic stem cell differentiation by altering the bone niche. Cell Metab 22: 886-894, 2015.

55. Zou W, Greenblatt MB, Brady N, Lotinun S, Zhai B, de Rivera H, Singh A, Sun J, Gygi SP, Baron R, *et al*: The microtubule-associated protein DCAMKL1 regulates osteoblast function via repression of Runx2. J Exp Med 210: 1793-1806, 2013.

56. Sureban SM, May R, Lightfoot SA, Hoskins AB, Lerner M, Brackett DJ, Postier RG, Ramanujam R, Mohammed A, Rao CV, *et al*: DCAMKL-1 regulates epithelial-mesenchymal transition in human pancreatic cells through a miR-200a-dependent mechanism. Cancer Res 71: 2328-2338, 2011.

57. Sureban SM, May R, Ramalingam S, Subramaniam D, Natarajan G, Anant S and Houchen CW: Selective blockade of DCAMKL-1 results in tumor growth arrest by a Let-7a MicroRNA-dependent mechanism. Gastroenterology 137: 649-659, 2009.

58. Cao T, Li H, Hu Y, Ma D and Cai X: miR-144 suppresses the proliferation and metastasis of hepatocellular carcinoma by targeting E2F3. Tumour Biol 35: 10759-10764, 2014.

59. Fan Y, Hanai JI, Le PT, Bi R, Maridas D, DeMambro V, Figueroa CA, Kir S, Zhou X, Mannstadt M, *et al*: Parathyroid hormone directs bone marrow mesenchymal cell fate. Cell Metab 25: 661-672, 2017.

60. Li JY, D'Amelio P, Robinson J, Walker LD, Vaccaro C, Luo T, Tyagi AM, Yu M, Reott M, Sassi F, *et al*: IL-17A is increased in humans with primary hyperparathyroidism and mediates PTH-induced bone loss in mice. Cell Metab 22: 799-810, 2015.